

## **Near-source effects on DAS recording: implications for tap tests**

B.L.N. Kennett(1), V.H. Lai(1), M.S. Miller(1), D. Bowden(2) & A. Fichtner(2)

*(1) Research School of Earth Sciences, The Australian National University,  
Canberra ACT 2601, Australia*

*(2) Department of Earth Sciences, ETH Zurich, Zurich, Switzerland*

Corresponding author: [Brian.Kennett@anu.edu.au](mailto:Brian.Kennett@anu.edu.au)

This is a Postprint updating the material at EarthArXiv after review and paper acceptance

It has been published in *Geophysical Journal International* with doi:  
<https://doi.org/10.1093/gji/ggae055>

submitted to *Geophys. J. Int.*

# Near-source effects on DAS recording: implications for tap tests

B.L.N. Kennett<sup>1</sup>, V.H. Lai<sup>1</sup>, M.S. Miller<sup>1</sup>, D. Bowden<sup>2</sup> & A. Fichtner<sup>2</sup>

<sup>1</sup> *Research School of Earth Sciences, The Australian National University, Canberra, Australia,*

*Email: (Brian.Kennett@anu.edu.au)*

<sup>2</sup> *Department of Earth Sciences, ETH Zurich, Zurich, Switzerland*

## SUMMARY

In the immediate vicinity of a source there are strong gradients in the seismic wavefield that are tamed and modified in DAS recording due to combined effects of gauge-length averaging and local stacking on the local strain field. Close to a source broadside propagation effects are significant, and produce a characteristic impact on the local DAS channels. In the presence of topography, of surface or cable, additional effects are introduced that modify the expected signal. All these influences mean that the results of tap tests used to calibrate the channel positions along a DAS cable may give a distorted view of the actual geometry. Such effects can be important for detailed mapping of faulting processes and comparable features.

**Key words:** Distributed acoustic sensing; Site effects; Wave propagation;

## 1 INTRODUCTION

Distributed acoustic sensing (DAS) exploiting fibre optic cables has become an important tool for providing dense sampling of the seismic wavefield. Although the responses at individual channels can often be treated as point observations they are derived from scattered returns from multiple laser pulses that provide local averages of strain rate. The gauge length employed for this averaging is typically of the order of 10 m to secure good signal to noise ratios, and many DAS systems also include internal

2 *B.L.N. Kennett, V.H. Lai, M.S. Miller, D. Bowden, A. Fichtner*

stacking around the channel point to enhance signal. When signals are slowly varying, the effect of the averaging and stacking is slight and the channel response is close to the actual strain rate. However, when the seismic wavefield is changing rapidly, as in the immediate location of a source, the channel response is a modified version of the true scenario.

Some applications of DAS systems have deployed their own fibre optic cables (e.g., Wang et al., 2016; Hudson et al., 2020, Fichtner et al., 2023) where the configuration is well controlled and shallow burial can be expected to give good ground coupling. However, many applications rely on the exploitation of unused fibres on existing cables used for telecommunications, termed ‘dark’ fibres (e.g., Ajo-Franklin et al., 2019, Nayak et al, 2021; Spica et al, 2021) where the general configuration may be known but the specific geometry needs to be calibrated. In this case, it is common to employ "tap tests" to associate DAS channels with specific locations at the surface. For such situations, where a concentrated source is positioned close to the cable, near source effects become important and can lead to distortion of the mapping between channel number and position. A further complication with dark fibres is that the precise mode of deployment is difficult to determine and for cable in conduit the coupling to the surrounding environment can change quite quickly. In an urban situation there can also be significant effects from the nature of the built environment, with inspection pits and other below-ground structures scattering and reflecting seismic waves.

We here look at the way in which the DAS recording system modifies the seismic wavefield in the neighbourhood of a source and show how with variable coupling effects there can be marked differences in the apparent response for similar configurations. Such differences are seen in DAS experiments at the Tidbinbilla satellite tracking station near Canberra in Australia and along a street in Bern, Switzerland. Although the dominant signal recorded by DAS systems is usually the strain rate along the cable, in near-source situations it is possible for perpendicular effects to become noticeable for a brief interval around the source location. Also, inclined surfaces or cables can introduce apparent horizontal forcing in addition to the vertical forcing expected in tap testing for DAS channel geometry. The interaction of varying along-cable and weak cross-cable effects produce a diversity of modified channel responses and complicate calibration of channel location.

## 2 DAS RECORDING EFFECTS

In the DAS system the scattered return signals from a sequence of laser pulses delivered by the DAS interrogator are analysed to produce a measure of the relative change in optical path length  $\Delta g/g$  over a gauge length  $g$  (see, e.g., Hartog 2017 - section 9.1.3.3). Optical fibres are made of fused silica glass, with relatively high rigidity, so that there is low sensitivity to normally incident seismic waves. A detailed analysis of the changes of optical path length due to fibre strain and associated dielectric

effects has been provided by Kushnikov (2016): for typical fibre optic properties the change in optical path length is related to the axial strain along the fibre  $\epsilon_{\parallel}$  and in the transverse direction  $\epsilon_{\perp}$ ,

$$\Delta g/g \approx 0.7\epsilon_{\parallel} - 0.2\epsilon_{\perp}. \quad (1)$$

For weak perpendicular strain  $\epsilon_{\perp}$  the Poisson effect enhances the apparent longitudinal strain and so  $\Delta g/g \approx 0.8\epsilon_{\parallel}$  for a typical Poisson's ratio for an optical fibre of 0.2.

Only when the axial strain is small relative to the transversal strain will the second term on the right-hand side of (1) become significant. This effect can occur when waves arrive broadside to the cable very close to a source. Even so the contrasts between the cable packing and the stiff optical fibres acts to reduce the effective transverse strain of the fibre compared with that impinging on the exterior of the cable. In favourable circumstances, the transversal fibre strain may reach about 5% of the transverse strain on the cable itself, but will generally be less.

The nature of the DAS signal depends on the orientation of the cable with respect to the passing seismic waves and the influence of gauge length effects. The specific nature of the gauge length averaging for each channel depends on the pulse form employed in the DAS interrogation (Parker et al., 2014).

The axial strain rate  $\dot{\epsilon}_{\parallel}$  is given by the spatial derivative of ground velocity resolved along the cable  $v_d$ , so that  $\dot{\epsilon}_{\parallel} = \partial v_d(s)/\partial s$ , in terms of distance along cable  $s$ . Under the assumption of uniform sampling along the gauge length  $g$ , the effect of averaging the cross-cable and along-cable strain rates around the reference point takes the form of integrals

$$\langle \dot{\epsilon}_{\perp} \rangle = \frac{1}{g} \int_{-g/2}^{g/2} ds \dot{\epsilon}_{\perp}(s), \text{ and } \langle \dot{\epsilon}_{\parallel} \rangle = \frac{1}{g} \int_{-g/2}^{g/2} ds \frac{\partial v_d(s)}{\partial s} = \frac{1}{g} [v_d(g/2) - v_d(-g/2)]. \quad (2)$$

The averaged along-cable strain rate  $\langle \dot{\epsilon}_{\parallel} \rangle$  can therefore, in principle, be obtained by differencing the ground velocity resolved along the cable  $v_d$  at the ends of the gauge length. For the cross-cable component  $\langle \dot{\epsilon}_{\perp} \rangle$  there is no analogue and direct integration is needed. In the examples that follow we employ numerical quadrature using a high accuracy Romberg scheme.

The spatial averaging due to the gauge length is compounded by channel stacking procedures built into the DAS interrogator system, which help to counteract optical fading issues due to net-zero optical scattering at some locations along the cable (Zhan, 2020 - Figure 2). Different approaches are employed by the various manufacturers of DAS systems. Here we use a simple stacking over 11 sub-channels disposed around the output channel. We consider throughout a gauge length of 10 m, with output channels every 2 m. The sub-channels used for stacking are at 0.25 m separation, so the stack spans 2.75 m.

The combination of gauge-length averaging and stacking acts to spread the apparent effect of any localised strain disturbance with a single sign (Figure 1). The effect of gauge length averaging is that

4 *B.L.N. Kennett, V.H. Lai, M.S. Miller, D. Bowden, A. Fichtner*

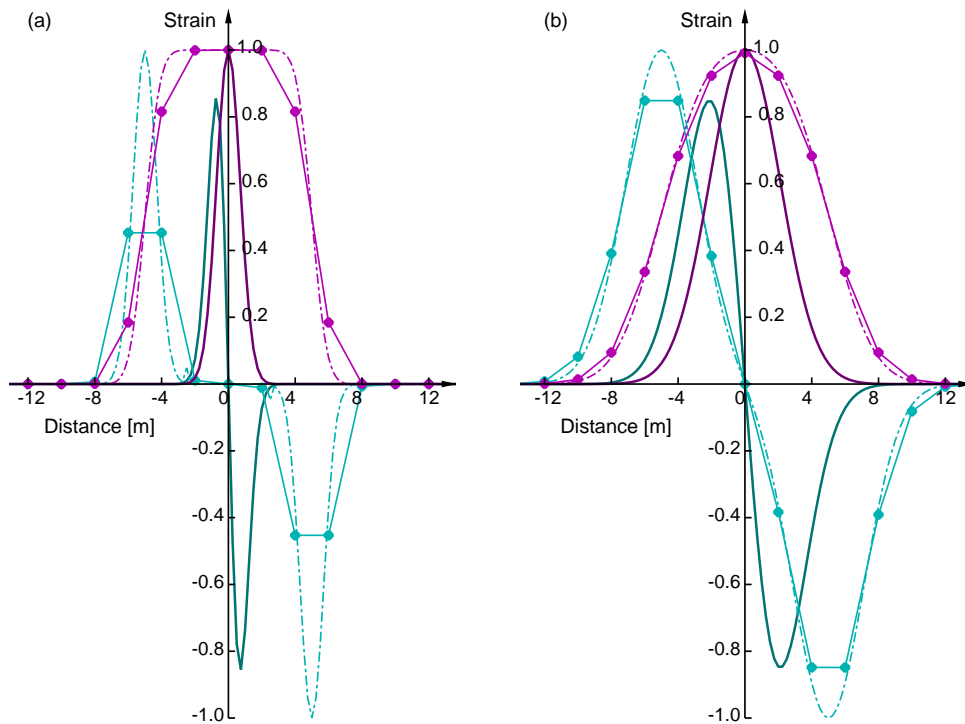


**Figure 1.** Influence of gauge length and instrumental averaging on simple signals with a narrow span: (a) half-width 1 m; (b) half-width 3 m. The input strain components are shown with solid lines, the effect of 10 m gauge length integration by chain dotted lines and finally the DAS output at channels separated by 2 m as solid lines with markers at the channels. This last stage includes instrumental stacking over 2.75 m around the output channel, combining 11 signals at 0.25 m separation. Magenta traces are for a symmetric strain signal about the origin, cyan traces for an antisymmetric strain signal

a concentrated strain signal will affect the output channels over at least the full gauge length. Further the shape of the response is only weakly dependent on the nature of the pulse as can be seen in the magenta traces in Figure 1(a),(b). For a ground velocity field that is symmetric about the origin, the strain will be antisymmetric. This antisymmetry is preserved in the gauge averaging, but rapid changes in pulse form are truncated by the stacking process (cyan traces in Figure 1a,b).

The action of the DAS system therefore imposes a characteristic modulation on strong localised signals that do not directly represent the strain (or strain-rate) at the cable. Another complication in terms of DAS records comes from variable coupling of the cable to ground motion, depending on the conditions of emplacement.

Further, within the cable there is a bundle of fibres, and the coupling to cable strain can depend to some extent on the specific configuration of the fibre used within the cable. Thus, where outward and inward paths are used with a fibre connection at the end of the cable away from the DAS interrogator,

different fibres will be in use and slight differences in DAS output at the same physical location can be expected.

The coupling of the cable to the surrounding medium also depends on the specific local conditions (e.g., Ajo-Franklin et al., 2019). For direct cable installation the conditions can be often be managed. However, where pre-existing cable is employed, as in the use of dark fibre, the nature of the emplacement is not under user control. For cable in near-horizontal conduit the effect of gravity and friction generally provides adequate coupling, though loop segments of spare cable may be present at inspection points.

The ambiguities of the physical geometry of the DAS cable being interrogated mean that calibration is need. This process is commonly accomplished with some class of “tap test” where a sharp force at a known location is applied and the DAS channels are mapped from the concentrated output signal. As we shall see the signals from such tap tests themselves show intriguing characteristics that can be tied to the configuration of the cable used for DAS recording and its physical surroundings.

Tap tests take place close to the DAS cable and so encounter the full-complexity of the seismic wavefield with both near and far-field terms. Nevertheless, useful indications of behaviour can be extracted using simple ray-based concepts coupled with the radiation from different sources, as developed in the Supplementary Material Section S1. We use expressions for the propagation of seismic waves in uniform media as a guide to the expected behaviour. Ground conditions along a DAS cable may well show variable heterogeneity in the near surface that will modify the wavefronts emitted from a source, but for short propagation distances the distortion will normally be limited and so the uniform medium behaviour will be a good approximation. In this way we obtain general results without needing to know the specific details of a complex model.

Where human-powered sources are used for tap-tests (e.g., jumping, sledgehammer blows or short weight drops) the local strains are modest and should lie well within the linear response range of the DAS system. Indeed, a common problem is that the energy imparted by such tap tests is too small to give an effective signal. For strong sources very close to a cable, such as an explosive charge or earthquake, it is likely that the optical fibres will respond non-linearly to the high strains with effects that can include frequency doubling. We do not consider such high-strain cases.

## **2.1 Cable below source**

When the DAS cable lies at some depth it may be possible to carry out tap tests almost directly above the cable. For this configuration it is possible to produce ray-based expressions for the strains induced by vertical or horizontal forcing; these are presented in Section S1.1 of the Supplementary Materials.

The dominant contribution to the DAS signal comes from the along-cable strain(-rate) component

6 *B.L.N. Kennett, V.H. Lai, M.S. Miller, D. Bowden, A. Fichtner*

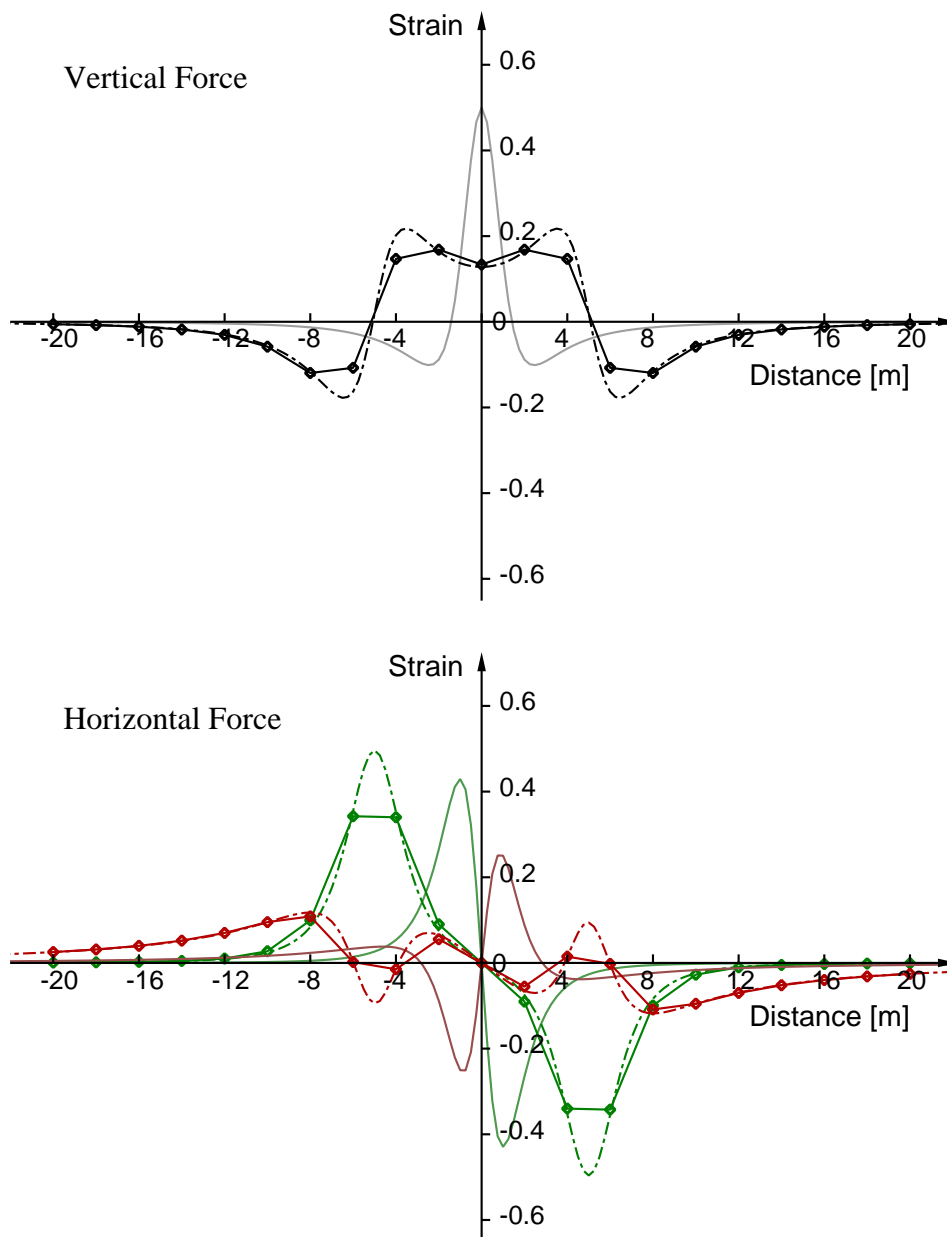


**Figure 2.** Along-cable behaviour of the DAS output for both P and S waves on a cable at 2 m depth from vertical and horizontal forcing. For a vertical force, the P and S behaviour is the same. For a horizontal force the P behaviour is shown in red and the S behaviour in green. The conventions for the traces follow Figure 1.

and so we will concentrate on this aspect and point out where transversal effects could also contribute. In Figure 2 we display the DAS output results using the ray-based expressions for a strain on a cable at 2 m depth. We show both the P and S wave components from vertical and horizontal forces applied immediately above the cable. The combination of the DAS orientation factors and the radiation patterns from the vertical force combine to give the same effective behaviour for both P and S waves.

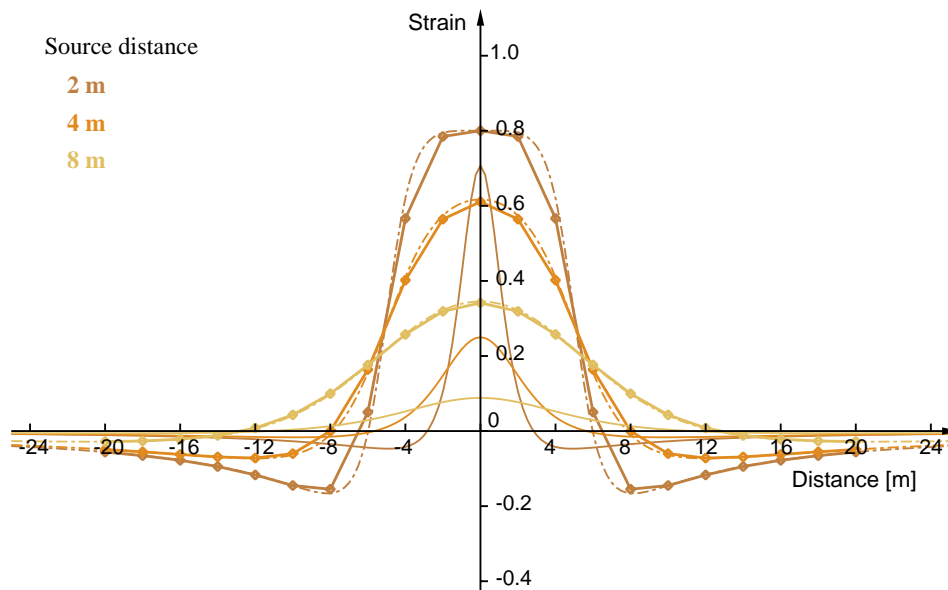


**Figure 3.** Along-cable behaviour of the DAS output for far-field Rayleigh waves for sources to the side at increasing distance from the cable. The conventions for the traces follow Figure 1.

As can be readily seen from Figure 2, the local DAS response to a vertical force is symmetric with sharp gradients in amplitude associated with the ends of the gauge length centred on the origin. Whereas, the contributions for both P and S waves from a horizontal force are anti-symmetric about the origin. The component transverse to the cable is symmetric and strongest in the presence of a horizontal force.

Even for a uniform medium a combination of the symmetric and anti-symmetric behaviour can produce a wide range of different behaviour depending on the balance of vertical and horizontal forces. Additional effects also arise from variable coupling of the DAS cable to its environment.

Horizontal forcing can arise from a direct impact, such as with a hammer, when the impact on the ground is not purely vertical. When the ground surface is sloping and the cable run follows the slope, a vertical impact on the surface will impart an apparent component along the cable, that can be described using a horizontal force.

## 2.2 Source to side of cable

A more common scenario in urban environments is where the cable is placed at a relatively shallow depth, e.g., under a road. In this case the feasible locations for conducting a tap tests are at the side of the road, e.g., by a jump on a sidewalk (see Section 4). This means that there is a surface source offset from the cable location, so that in addition to P and S body waves there will be Rayleigh waves. For such a situation it is not possible to produce any simple analytic representation of the strain signal

8 *B.L.N. Kennett, V.H. Lai, M.S. Miller, D. Bowden, A. Fichtner*

impinging on the cable. Nevertheless some general considerations can be extracted, as discussed in Section S1:2 of the Supplementary Materials.

For the body wave component the effect of the DAS system (Figure S6) is similar to that shown in Figure 2 for a vertical force, with segments of reversed sign bordering a central peak whose width is approximately the gauge length. Such features can be seen in the DAS synthetics for near-offset records in a layered medium presented by Kennett (2022).

For a close cable the Rayleigh wave field is not fully developed except for the highest frequencies. Even so we can gain a good idea of the behaviour by looking at the far-field scenario with radial distance dependence from the source  $r^{-1/2}$ . In Figure 3 we show the along-cable DAS signal for source separations of 2, 4 and 8 m from the cable. In each case the channel response is localised in the neighbourhood of the source, extending over no more than two gauge lengths. The weak contribution from transverse strain to the cable will tend to damp the polarity reversals. Longer path lengths can arise in an urban environment for reflections from below-ground structures such as cellars giving rise to a virtual source beyond the reflector.

### 3 EXPERIMENT AT TIDBINBILLA TRACKING STATION, CANBERRA

As an example of a situation with a buried cable at some depth we show results from the use of dark fibre at the Tidbinbilla Deep Space Tracking Station south of Canberra in Australia. The DAS system was attached to a loop of spare fibres in the cable leading from the central building to the north to a temporarily unused antenna dish. Data were collected using a Silixa iDAS interrogator with 2 m channel spacing and a 10 m fixed gauge length and 1000 Hz sampling rate. The length of cable was approximately 1.9 km. The experimental configuration is detailed in Section 2.1 of the Supplementary Material including a map of the site and cable layout.

The cable is placed in conduit at a nominal depth of 2 m below ground surface, with calibration "taps" at the surface, so that the source lies about 2 m away from the closest part of the DAS cable. The cable path follows a set of straight-line segments with some sharp changes of direction at inspection points. The surface conditions vary, with ground disturbance in places associated with past building work. The ground surface is undulating with some quite steep slopes in part.

The operations at the site, including reorientation of antenna dishes, generate significant low frequency noise but this is not a problem for the tap tests considered here. At regular points along the mapped cable path tests were conducted using either a set of sledgehammer blows or a vertical drop of a 2 kg tamper by about 60 cm. The records from the two different types of source were very similar.

The DAS records from the various tap tests display a range of behaviour, with some intriguing

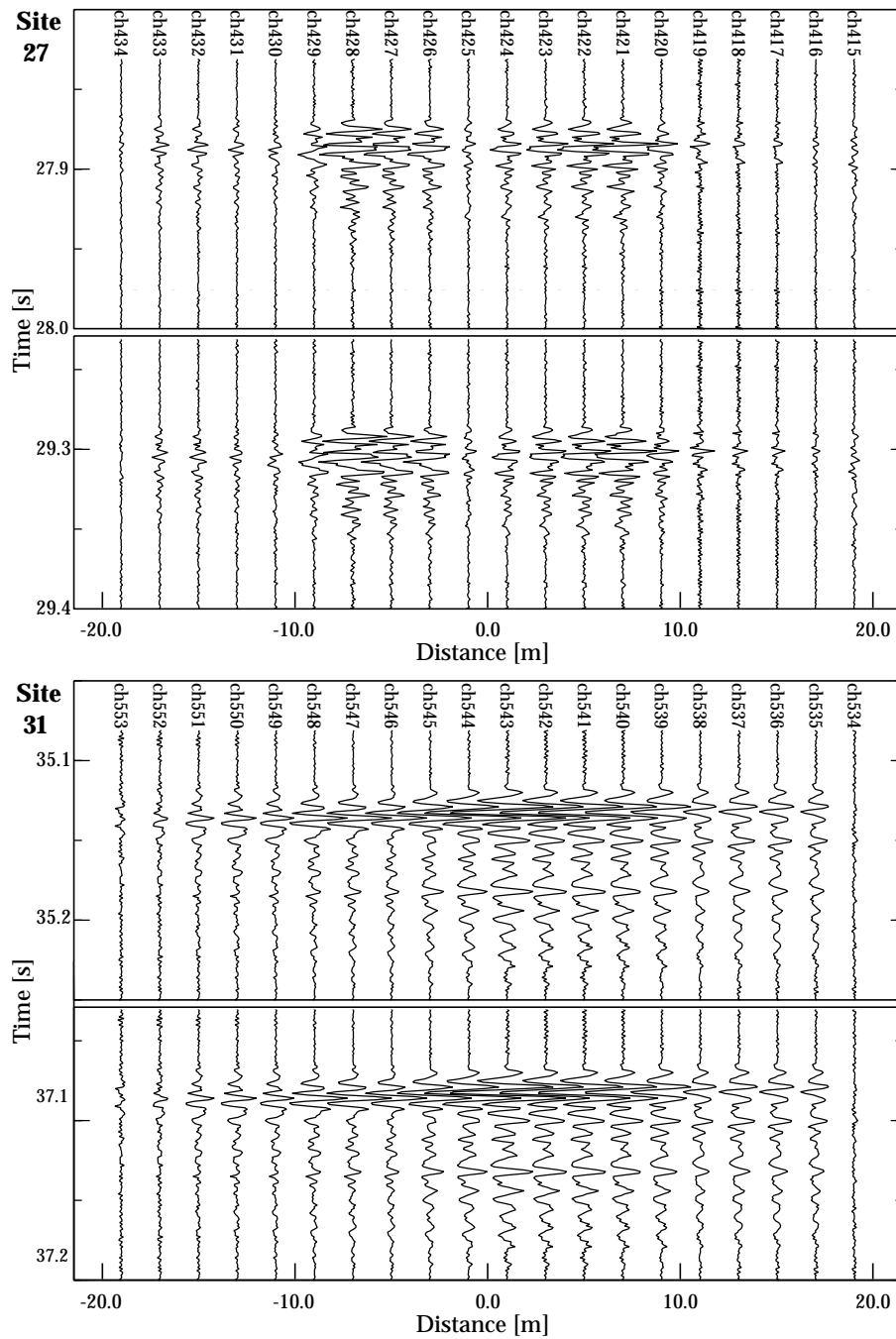


**Figure 4.** DAS records for tap tests at sites 27 and 31 at Tidbinbilla, with a weight drop source about 2 m above the DAS cable. For each site, two separate weight drops are illustrated to show the reproducibility of the response. The data are plotted at the original 1000 Hz sampling.

properties (e.g., Figures 4, 5). Such features are site specific and are reproducible with multiple source impacts. Comparable results are recorded on the inward and outward fibres.

For the weight drop source we would not expect to see DAS signals with the clear change in polarity apparent in site 27, with two separate weight drops illustrated. This site lies on a rather steep

10 *B.L.N. Kennett, V.H. Lai, M.S. Miller, D. Bowden, A. Fichtner*

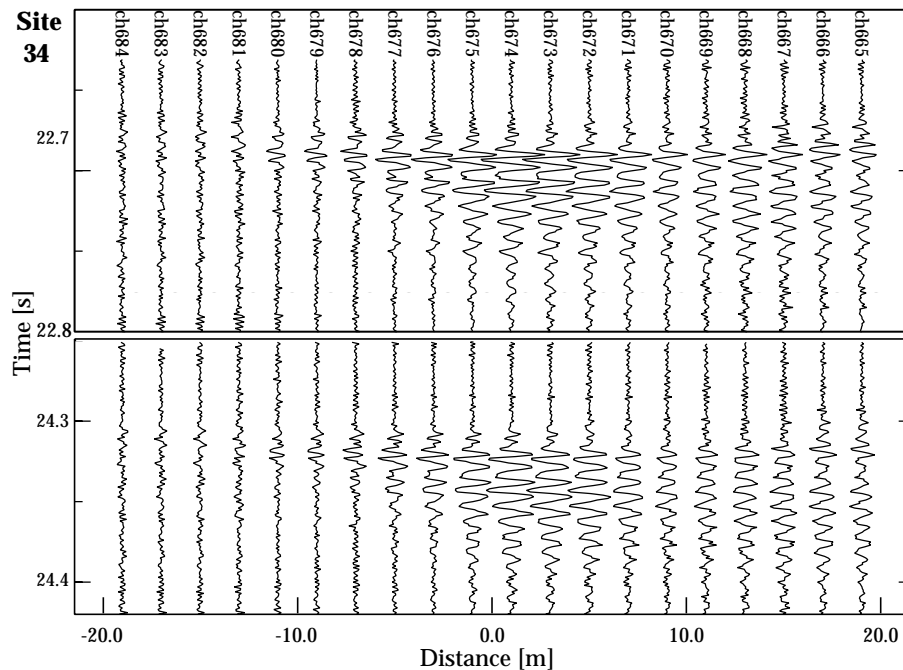


**Figure 5.** DAS records for tap tests at site 34 at Tidbinbilla, with again a weight drop source about 2 m above the DAS cable. Two separate weight drops are illustrated to show the reproducibility of the response. The data are plotted at the original 1000 Hz sampling, and the trace amplification is twice that used for the traces in Figure 4 at sites 27 and 31.

incline leading up to a road to one of the antennas (Figure S8) and it is presumed that the cable conduit follows the slope. In this condition the vertical impact will generate components perpendicular to and along the cable run, corresponding to the vertical and horizontal forces in Figure 2. It would appear that the anti-symmetric effect of the component along the cable dominates at site 27, so that we see P waves from horizontal forcing. The trace with the smallest amplitude, just at the polarity reversal, will represent the closest point on the cable to the tap test. However, this will not lie vertically beneath the calibration point!

At site 31, which is on a mild slope the records show a rather different character. There is noticeable asymmetry in the propagation characteristics with a sharp cut-off at ch534 that can be associated with strong ground disturbance near an access pit. At each end of the main zone of high amplitude there is a rapid drop in amplitude. Such strong gradients are consistent with the general behaviour expected for a vertical force, from Figure 3, though the highest amplitudes persist to slightly greater distance than for the simple ray-based predictions.

In general, the channel with the earliest arrival can be expected to be that which is closest to the source. However, contrasts in local ground properties can make such identification difficult. Often the

onset of the tap signal is not very clear, so that it can be difficult to determine the channel with the first arrival, in part because the internal averaging in DAS units tends to smear out the wavefronts.

An example is shown in Figure 5, for site 34 about 100 m beyond site 31 shown in Figure 4. With the same style of source input the DAS signal was much lower so the traces are plotted with twice the amplification used in Figure 4. The DAS records show even stronger differences between the two sides of the shot point than for site 31. The stronger reverberations for smaller channel numbers suggest some change in the cable coupling or ground properties. The onsets on the traces are not easy to pick because of the small signal but indicate the likelihood of reduced wavespeed near the tap test point. It is possible to make a reasonable guess for the calibration point at ch674, but the uncertainty is several channels.

#### **4 EXPERIMENT ON BERN STREETS, SWITZERLAND**

As an example of a test in an urban environment we consider a pilot experiment conducted in Bern, Switzerland that used the DAS system on unused fibres on a telecommunication cable connecting educational institutions about 2 km apart (access provided by the SWITCH foundation). The fibre optic cable is reported to be housed in a plastic conduit, buried at a depth of  $\sim 0.7$  m beneath the surface of the road. During construction, this conduit was covered with sand before the road surface was laid on top. The experimental configuration is detailed in Section 2.2 of the Supplementary Material, including a map of the layout.

The DAS layout consisted of  $\sim 3$  km of cable in a T-configuration, with the signal reflected at the far end, resulting in signal measured over  $\sim 6$  km of fibre, with repeating sections. Data were collected using a Silixa iDAS Version 2.4 interrogator, 2 m channel spacing and a 10 m fixed gauge length. Data are plotted with a 200 Hz sampling rate.

Calibration of the cable geometry was carried out with a set of jumps at regular intervals along the sidewalk bordering the roads under which the cable was laid. The precise position of the cable under the road is not known, but the jump sites should lie no more than 2-3 m from the cable. For most jump locations the seismic energy produced propagated to considerable distances (more than 40 m away from the source). The wavefield characteristics are also very consistent between jumps at the same point.

From the ensemble of jump records from this Bern experiment, Kennett (2022) was able to produce a simple 1-D layered model with depth for which synthetic DAS records provide a good description of the further offset behaviour. However, on most records there were prominent features near the jump sites that could not be explained by the layered model. Examples are shown in Figures 6, 7, which both show significant coda over a narrow span of DAS channels.

12 *B.L.N. Kennett, V.H. Lai, M.S. Miller, D. Bowden, A. Fichtner*

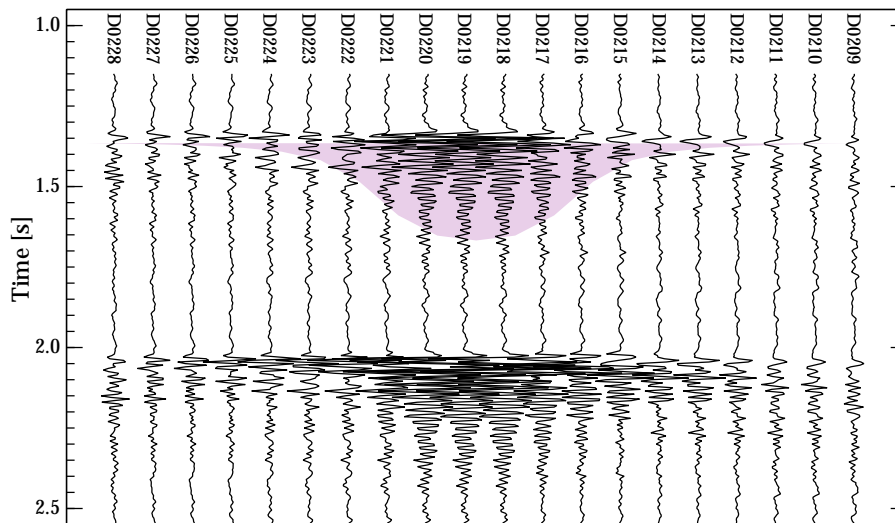


**Figure 6.** DAS records for multiple jumps at Site A in Bern, lying about 2 m away from the DAS cable. The shaded area indicates the expected length of coda for the broadside contribution to Rayleigh waves.

The records in Figure 6 are for jump point A on a straight section of street with a narrow sidewalk bordered immediately by buildings. The other side of the road has a cycle track and then woodland. The jump energy extends to considerable distance with a relatively compact refracted wave packet and clear indications of a layered structure in depth. Yet, for the channels nearest the jump there is a noticeable coda with frequency of 40 Hz or more extending for more than 0.3 s. This feature is seen for multiple jumps and so is representative of this site. The character of the coda is suggestive of Rayleigh waves travelling in a very thin near-surface waveguide with strong group dispersion. The strong interaction of multiple wave contributions near the jump point makes it difficult to extract amplitude information directly. However, the length of the coda acts as an effective proxy for the peak amplitude of the developing surface waves. Thus, in Figure 6 we have superimposed the expected behaviour for an offset source for a decay slightly slower than for far-field Rayleigh waves. For short distances the full far-field decay is not exhibited.

Jump point B is along another straight road segment but now with a more complicated built environment. The road is wider (about 12 m) bordered on each side by sidewalks abutting substantial buildings with cellars. Away from the jump point the orientation of buildings is more complex with some set away from the road. The DAS records for two jumps at this site are shown in Figure 7 and each displays a strong amplitude arrival behind the body waves followed by distinct later pulses with a similar distance span. The pattern of arrivals would be consistent with an initial Rayleigh wave contribution reflected from the building behind the jump point near the kerb, followed by Rayleigh waves that have been reflected back from below-ground structure on the other side of the road. The

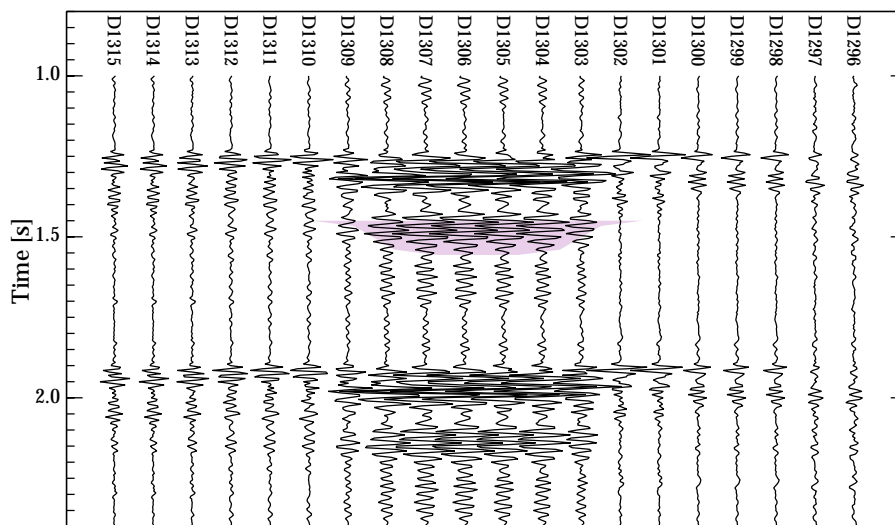


**Figure 7.** DAS records for multiple jumps at Site B in Bern, again lying about 2 m away from the DAS cable. The shaded area highlights the spatial extent of the late coda most likely due to reflected Rayleigh waves from below-ground structures at the sides of the street.

reflectors will have the effect of creating virtual sources with longer path lengths to the DAS cable, for which the recorded strain contribution will still be confined near the jump point (Figure 3). We have marked in Figure 7 the expected span for such later arrivals and this matches well with the observations. The geometry for such reflections is illustrated in Section S3 of the Supplementary Materials.

For both sets of jumps we see a noticeable modulation of the amplitude of the first arriving body waves of the style seen in Figure 2. Such behaviour with possible polarity reversals is predicted for far-field body waves (Figure S6). Some weak influence of strain contributions transverse to the cable may also be present. The modulation patterns for a uniform medium will be symmetric about the source point, but can be affected by lateral variations in ground properties. Such patterns can be useful in tying down the calibration of DAS channels.

The complex streetscape in the Bern experiments, particularly below ground, gives rise to a range of different behaviour depending on the built environment close to the source. At each jump point the dominant effects are found in the narrow distance span around the jumps illustrated in Figures 6 and 7, though in a few cases some wide-angle horizontal reflection may be present.

## 5 ALTERNATIVE DAS CABLE CALIBRATION

With improvements in DAS technology it has become possible to obtain effective recordings for many tens of kilometres using dark fibres from telecommunication cables. Calibration of such lengths with

14 *B.L.N. Kennett, V.H. Lai, M.S. Miller, D. Bowden, A. Fichtner*

conventional tap testing, as discussed above, would be very onerous, but is necessary to identify cable loops and comparable zones where signal is degraded.

Typically such cables lie under or in close proximity to roads and this offers the chance of using the DAS signal generated by a passing vehicle for calibration. The broad frequency response of DAS systems allows the simultaneous recording of the quasi-static strain response due to the weight of the vehicle and the seismic waves produced by the moving source (e.g., Yuan et al. 2020). The strain rate produced by the weight of a car moving at speeds slower than the surface Rayleigh waves is highly localised and readily allows the identification of the closest DAS channels to within a gauge length. The quasi-static strain rate signal is strongly expressed below 1 Hz and can be separated from the seismic waves generated by the passage of the vehicle by low-pass filtering.

With the aid of a vehicle using real-time tracking with GNSS (Global Navigation Satellite System) that also provides a common time base for the car and the DAS recording system, the low-frequency quasi-static signal can be exploited to calibrate kilometres of cable (Biondi et al. 2022). The basic assumption is that the strongest signal will occur at the closest DAS channel location, which will work well with shallow cable emplacement if the car is driven on the same part of the road as where the cable is located. The efficacy of the process depends to some extent on the quality of mapping of the original fibre layout, so that the car can travel on the segment of the road closest to the cable line.

## 6 DISCUSSION AND CONCLUSIONS

In the immediate vicinity of a source there are inevitably rapid variations in the nature of the seismic wavefield that are tamed and somewhat modified by a DAS recording system. In particular, there are significant contributions from waves that arrive nearly broadside to the cable containing the optical fibre being exploited for sensing. Most contribution comes from along-cable strain but can be augmented slightly by cross-cable effects. The action of the gauge length averaging and subsequent stacking in the DAS system mean that the net effect near the source depends weakly on the specifics of the distance from the source to the cable.

For experiments using a cable in conduit at modest depth, the direct DAS response to a typical near-vertical force is not strong. As a result where the ground surface is sloping with constant conduit depth, or where the conduit itself changes its depth apparent horizontal forcing can be present that significantly modifies the appearance of the records. Calibration of DAS channels from tap testing is unlikely to be more accurate than 2-3 channels when variations in ground properties and surface topography are taken into consideration.

For the more common scenario for dark fibres in existing telecommunication cables emplaced at a shallow depth beneath a road, tap testing will normally be offset from the cable. A characteristic

pattern of variations in amplitude in the first arrivals can help to pin down the span of the gauge length and hence the most likely calibration point. Over the same interval there can also be significant contributions from near broadside arrivals that leave a distinct local coda in the records.

Given the potential ambiguities in calibrating a DAS cables with widely spaced tap tests, using two taps within a gauge length may be helpful to bracket position and provide some measure of uncertainty. Where cables have sharp bends, recordings of distant events will show a change of character at the bend location (see, e.g., Kennett, 2022) and again provide a constraint on the mapping of cable channels as a supplement to tap tests.

The broad frequency response of DAS recording systems means that both quasi-static and wave propagation effects from a source can contribute to the observed signal. In the case of a moving vehicle, the low-frequency strain-rate effects due to the steady movement of the car's weight are the strongest and so are the most effective for calibration to at least a gauge length. Without any movement of the source, near-source deformation produces only minor effects and the dominant strain-rate signal comes from the seismic waves generated by the source.

The action of gauge-length and stacking effects is to broaden the zone of highest amplitude DAS signal in the neighbourhood of the source location, as we have seen for simple human-powered sources. Depending on the particular type of instrumentation employed, strong near-cable sources can produce strain-rates such that the optical phase of the returned pulse cannot be correctly measured and hence the apparent DAS signal is distorted ("clipping"). This effect is most likely when the differential phase is close to  $\pi$  or  $-\pi$ , because of the  $2\pi$  ambiguity in phase. Katakami et al. (2024) demonstrate such effects on isolated channels from a Mj 6.6 earthquake near Kyushu, Japan recorded on a DAS cable at 150 km distance, the net result is aliasing with spurious high frequency signals. In this case, with an occasional effect, it can be corrected by extrapolating from nearby unaffected channels. However, clipping is likely to pose a serious issue when many contiguous channel locations are affected.

## ACKNOWLEDGEMENTS

This project was partially supported by an ACR Future Fellowship (FT210100440) to MSM, and ARC Discovery Grant (DP230100277) – MSM, VHL, AF. The Australian field component was enabled in part by AuScope and the Australian Government via the National Collaborative Research Infrastructure Strategy (NCRIS): auscope.org.au. The Swiss component was supported by European Union Horizon 2020 research and innovation program under Grant Agreement 821115; *Real-Time Earthquake Risk Reduction for a Resilient Europe* (RISE), and Eidgenössische Technische Hochschule (ETH) Zürich.

16 *B.L.N. Kennett, V.H. Lai, M.S. Miller, D. Bowden, A. Fichtner*

For fieldwork assistance we thank Robert Pickle and Herb McQueen at Tidbinbilla, and Krystyna Smolinski in Bern. We are grateful to CSIRO, the operators of the Canberra Deep Space Communication Complex, for access to the optical fibre at Tidbinbilla. Thanks also to Felix Kugler from the SWITCH Foundation who provided access to the cable in Bern.

### Data access

The SAC records for the various tap tests are available at Zenodo (<https://doi.org/10.5281/zenodo.10258022>), along with the software for calculating the DAS response for different source configurations.

### REFERENCES

- ACTmapi, 2023. Australian Capital Territory interactive mapping, ACT Government, Canberra, Australia: <https://www.actmapi.act.gov.au>
- Aki, K. & Richards, P.G., 1980. *Quantitative Seismology*, W.H. Freeman, San Francisco.
- Ajo-Franklin, J.B., Dou, S., Lindsey, N.J., Monga, I., Tracy, C., Robertson, M., Tribaldos, V.R., Ulrich, C., Freifeld, B., Daley, T. & Li X., 2019. Distributed acoustic sensing using dark fibre for near-surface characterization and broadband seismic event detection. *Scientific Reports*, **9**(1), 1–14. doi: 10.1038/s41598-018-36675-8
- Biondi, E., Wang, X., Williams, E.F. & Zhan, Z., 2023. Geolocalization of large-scale DAS channels using a GPS-tracked moving vehicle. *Seism. Res. Lett.*, **94**, 318–330. doi: 10.1785/0220220169
- Fichtner, A., Hofstede, C., Kennett, B.L.N., Nymand, N.F., Lauritzen, M.L., Zigone, D. & Eisen, O., 2023. Fiber-optic airplane seismology on the Northeast Greenland Ice Stream, *The Seismic Record*, **3**(2), 125–133. doi: 10.1785/0320230004
- Hartog, A. H., 2017. *An Introduction to Distributed Optical Fibre Sensors*, CRC Press, Boca Raton, FL.
- Hudson, T.S., Baird, A.F., Kendall, J.-M., Kufner, S.K., Brisbourne, A.M., Smith, A.M., Butcher, A., Chalari, A. & Clarke, A., 2021. Distributed acoustic sensing (DAS) for natural microseismicity studies: a case study from Antarctica, *J. Geophys. Res.: Solid Earth*, **126**, e2020JB021493. doi: 10.1029/2020JB021493
- Katakami, S., Noda, S., Korenaga, M., Araki, E., Takahashi, N., & Iwata, N., 2024. Potential of earthquake strong motion observation utilizing a linear estimation method for phase cycle skipping in distributed acoustic sensing. *J. Geophys. Res.: Solid Earth*, **129**, e2023JB027327. doi: 10.1029/2023JB027327
- Kennett, B.L.N., 1983. *Seismic Wave Propagation in Stratified Media*, Cambridge University Press.
- Kennett, B.L.N., 2022. The seismic wavefield as seen by distributed acoustic sensing arrays: local, regional and teleseismic sources. *Proc. R. Soc. A*, **478**, 20210812. doi: 10.1098/rspa.2021.0812
- Kuvshinov, B., 2016. Interaction of helically wound fibre-optic cables with plane seismic waves, *Geophysical Prospecting*, **64**, 671–688. doi: 10.1111/1365-2478.12303

- Nayak, A., Ajo-Franklin, J.B. & the Imperial Valley Dark Fiber Team, 2021. Distributed acoustic sensing using dark fiber for array detection of regional earthquakes, *Seismol. Res. Lett.* **92**, 2441–2452, doi: 10.1785/0220200416
- Paitz, P., Edme, P., Gräff, D., Walter, F., Doetsch, J., Chalari, A., Schmelzbach, C. & Fichtner, A., 2020. Empirical investigations of the instrument response for distributed acoustic sensing (DAS) across 17 Octaves, *Bull. Seismol. Soc. Am.* **111**, 1–10. doi: 10.1785/0120200185
- Parker, T., Shatalin, S. & Farhadiroushan, M., 2014. Distributed Acoustic Sensing – a new tool for seismic applications, *First Break*, **32**, 61–69, doi: 10.3997/1365-2397.2013034
- Spica, Z.J., Perton, M., Martin, E.R., Beroza, G.C. & Biondi, B., 2020. Urban seismic site characterization by fiber-optic seismology. *J. Geophys. Res. Solid Earth*, **125**, 1–14. doi: 10.1029/2019JB018656
- Yuan, S., Lellouch, A., Clapp, R.G. & Biondi, B., 2020. Near-surface characterization using a roadside distributed acoustic sensing array. *The Leading Edge*, **39**(9), 646–653. doi: 10.1190/tle39090646.1
- Zhan, Z., 2020. Distributed acoustic sensing turns fiber-optic cables into sensitive seismic antennas, *Seismol. Res. Lett.*, **91**, 1–15. doi: 10.1785/0220190112

*Geophys. J. Int.*

## Near-source effects on DAS recording: implications for tap tests

B.L.N. Kennett<sup>1</sup>, V.H. Lai<sup>1</sup>, M.S. Miller<sup>1</sup>, D. Bowden<sup>2</sup> & A. Fichtner<sup>2</sup>

<sup>1</sup> Research School of Earth Sciences, The Australian National University, Canberra, Australia,

*Email: (Brian.Kennett@anu.edu.au)*

<sup>2</sup> Department of Earth Sciences, ETH Zurich, Zurich, Switzerland

### SUPPLEMENTARY MATERIALS

#### 1 SOURCE EFFECTS ON DAS CABLES

Under the assumption of uniform sampling along the gauge length  $g$ , the effect of averaging the axial strain rate around the reference point takes the form of integrals of strain rate

$$\langle \dot{\epsilon}_{\perp} \rangle = \frac{1}{g} \int_{-g/2}^{g/2} ds \dot{\epsilon}_{\perp} \text{ and } \langle \dot{\epsilon}_{\parallel} \rangle = \frac{1}{g} \int_{-g/2}^{g/2} ds \frac{\partial v_d(s)}{\partial s} = \frac{1}{g} [v_d(g/2) - v_d(-g/2)] \quad (1)$$

The averaged along-cable strain rate can therefore, in principle, be obtained by differencing the ground velocity resolved along the cable  $v_d$  at the ends of the gauge length. For the cross-cable component there is no analogue and direct integration is needed. Many DAS systems also include local stacking to enhance signals and in the examples below 11 signals at 0.25 m separation, spanning 2.75 m, are combined around the output channel.

We can gain insight into the behaviour expected in the neighbourhood of the source by using ray-based expressions for the strain produced by different force systems and then subjecting these results to gauge-length averaging and stacking. We consider a uniform medium characterised by P wacvespeed  $\alpha$ , S wavespeed  $\beta$  and density  $\rho$ . We use a far-field formulation, though the short distances involved in most experiments for DAS cable calibration will mean that near-field terms could also be important.

We consider two different styles of configuration of source and DAS cable. In Section S1.1 we look at a source above a cable, with a wavefield dominated by body waves, where the inclination of the wavefront plays an important role. In Section S1.2 we consider the more common case for

2 *B.L.N. Kennett, V.H. Lai, M.S. Miller, D. Bowden, A. Fichtner*

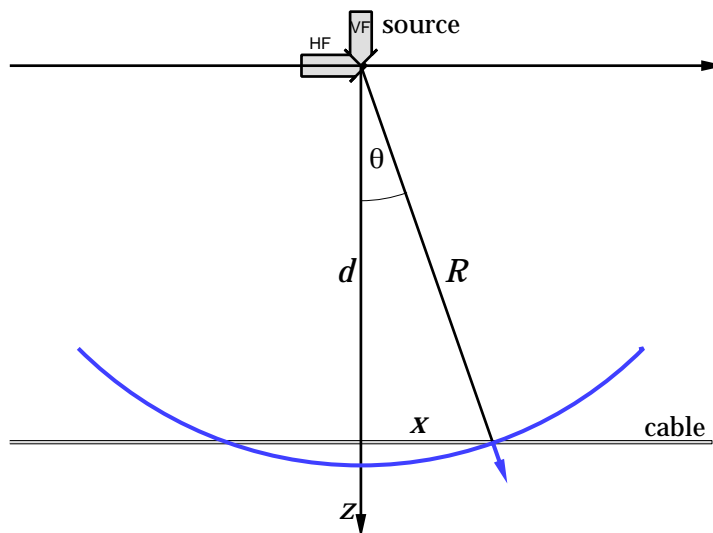


**Figure S1.** Configuration of subsurface cable at depth  $d$  with source at the origin.

DAS channel calibration with a shallow cable and an offset source, where Rayleigh surface waves are significant in addition to body waves.

### 1.1 Cable below source

We illustrate the combined effects of DAS gauge length and local stacking for the strain field measured on a horizontal cable at some depth  $d$  below the source (Figure S1). We consider the effects of both horizontal and vertical forces operating in an unbounded medium concentrating on the dominant far-field terms for P and S waves whose displacement diminishes as  $R^{-1}$  with radial distance  $R$  from the source origin.

For a point along the cable a distance  $x$  from the origin,  $R = (d^2 + x^2)^{1/2}$  and the angle to the vertical  $\theta = \tan^{-1}(x/d)$ . Thus  $\cos\theta = d/R$  and  $\sin\theta = x/R$ .

For a vertical force the ground velocity field for P and S waves takes the form (Aki & Richards, 1980; )

$$\mathbf{v}_{VF}^P = \frac{1}{4\pi\rho\alpha^2 R} [\sin\theta \cos\theta, \cos^2\theta], \quad \mathbf{v}_{VF}^S = \frac{1}{4\pi\rho\beta^2 R} [\sin\theta \cos\theta, -\sin^2\theta], \quad (2)$$

and for a horizontal force along the  $x$ -direction

$$\mathbf{v}_{HF}^P = \frac{1}{4\pi\rho\alpha^2 R} [\sin^2\theta, \sin\theta \cos\theta], \quad \mathbf{v}_{HF}^S = \frac{1}{4\pi\rho\beta^2 R} [\cos^2\theta, -\sin\theta \cos\theta]. \quad (3)$$

In terms of the horizontal coordinate  $x$  the expressions for a vertical force are

$$\mathbf{v}_{VF}^P = \frac{1}{4\pi\rho\alpha^2 (d^2 + x^2)^{3/2}} [xd, d^2], \quad \mathbf{v}_{VF}^S = \frac{1}{4\pi\rho\beta^2 (d^2 + x^2)^{3/2}} [xd, -x^2], \quad (4)$$

and for a horizontal force along the  $x$ -direction

$$\mathbf{v}_{HF}^P = \frac{1}{4\pi\rho\alpha^2 (d^2 + x^2)^{3/2}} [x^2, xd], \quad \mathbf{v}_{HF}^S = \frac{1}{4\pi\rho\beta^2 (d^2 + x^2)^{3/2}} [d^2, -xd]. \quad (5)$$

Differentiating with respect to depth and horizontal position we can construct the vertical strain  $e_{zz}$  and the strain along the cable  $e_{xx}$ . For the vertical force

$$[e_{xx}, e_{zz}]_{VF}^P = \frac{1}{4\pi\rho\alpha^2(d^2 + x^2)^{5/2}} [d(d^2 - 2x^2), -d(d^2 - 2x^2)], \quad (6)$$

$$[e_{xx}, e_{zz}]_{VF}^S = \frac{1}{4\pi\rho\beta^2(d^2 + x^2)^{5/2}} [d(d^2 - 2x^2), -3dx^2], \quad (7)$$

and for the horizontal force

$$[e_{xx}, e_{zz}]_{HF}^P = \frac{1}{4\pi\rho\alpha^2(d^2 + x^2)^{5/2}} [x(2d^2 - x^2), -d(x^2 - 2d^2)], \quad (8)$$

$$[e_{xx}, e_{zz}]_{HF}^S = \frac{1}{4\pi\rho\beta^2(d^2 + x^2)^{5/2}} [-3xd^2, d(x^2 - 2d^2)], \quad (9)$$

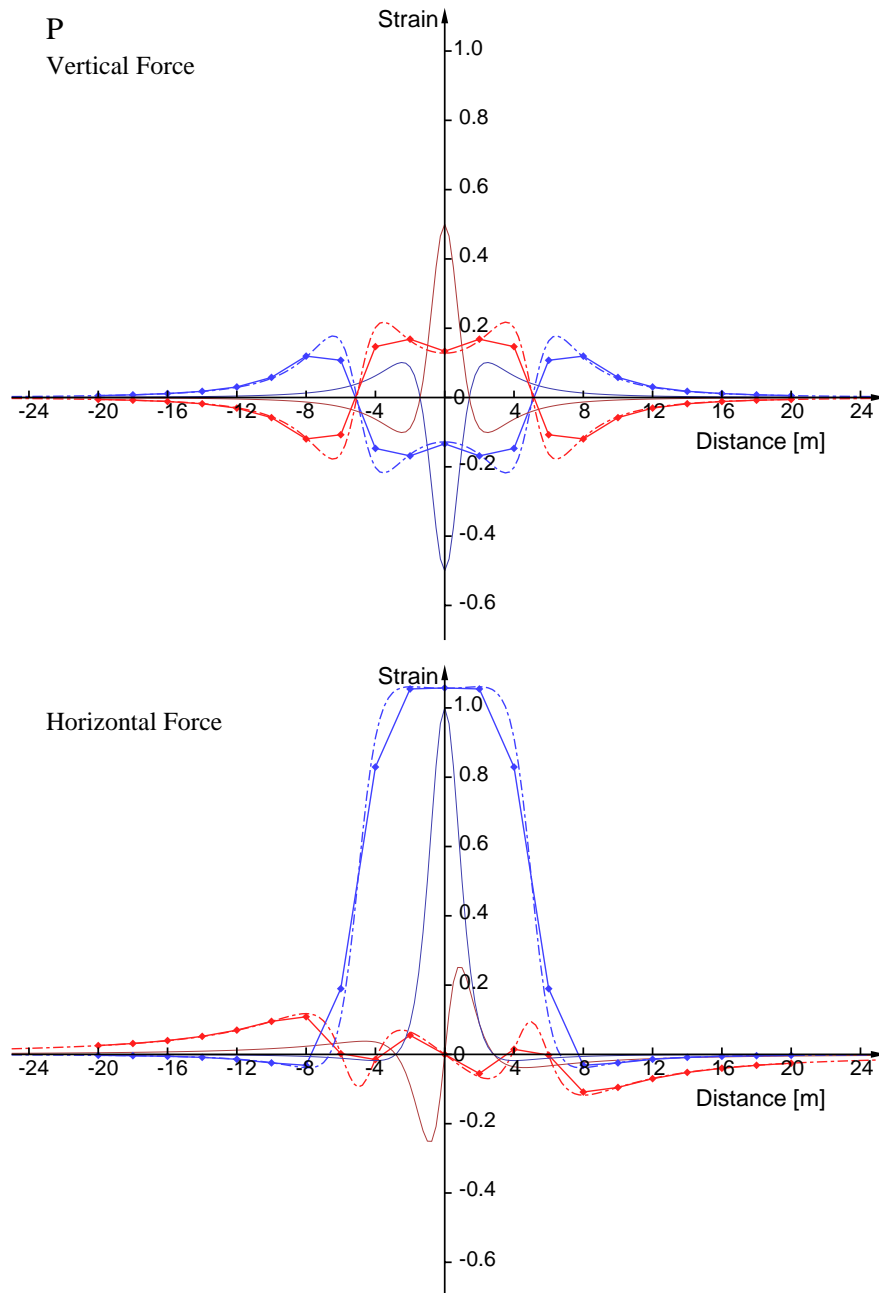
These strain fields are displayed in Figures S2 and S3 for P and S waves, together with the effects of DAS recording. The vertical strain  $e_{zz}$  is shown with a blue solid line and the horizontal strain  $e_{xx}$  with a red solid line. To extract the DAS signal the strains are integrated over the gauge interval at 0.25 m spacing, assuming uniform sampling. The integrals are evaluated numerically using a high-accuracy Romberg integration scheme. The averaged strains are shown by chain-dotted lines using the same colour convention as before. To simulate internal stacking effects, the averaged strains are then stacked over 2.75 m around the output channel, combining 11 signals at 0.25 m separation. This DAS output is indicated with markers at the 2 m channel interval connected by solid lines.

As can be seen from Figures S2 and S3, the effect of averaging over the gauge length substantially modifies the signal. Any narrow spike will be picked up by the integration over a full gauge length and so appear to have a width close to the gauge length. The shape of output is only weakly dependent on the specific shape of the original strain. As a result, the strong horizontal signal due to a horizontal force is very similar for a smaller cable depths (e.g., 1 m). There is less effect from stacking except where the averaged strain varies rapidly.

For the P wave case (Figure S2) the action of a vertical force produces a weak signal at depth even for the horizontal component directed along the cable. For a horizontal force, the along-cable component is strong whilst the cross-cable strain remains small.

For S waves (Figure S3) the horizontal response is the same as for P for a vertical force, but the averaged cross-cable component is larger. For a horizontal force, the along-cable component shows a change of sign as the source location is passed, whereas the cross-cable component is symmetric about the origin.

For a source imposed at the surface of a half space, the situation is more complicated. Nevertheless, for downgoing waves the full-space results provide a good approximation for a cable at depth for moderate offsets from the source.

4 *B.L.N. Kennett, V.H. Lai, M.S. Miller, D. Bowden, A. Fichtner*

**Figure S2.** P wave DAS fields for a cable at 2 m depth with vertical and horizontal forces imposed at the origin. Along-cable results for  $e_{xx}$  are shown in red and cross-cable for  $e_{zz}$  in blue. The actual strain components are shown with light solid lines, the effect of 10 m gauge length integration by chain dotted lines and the DAS output at channels separated by 2 m with markers at the channels. This last stage includes instrumental stacking over 2.75 m around the output channel, combining 11 signals at 0.25 m separation.

## Near-source effects on DAS recording: SM 5

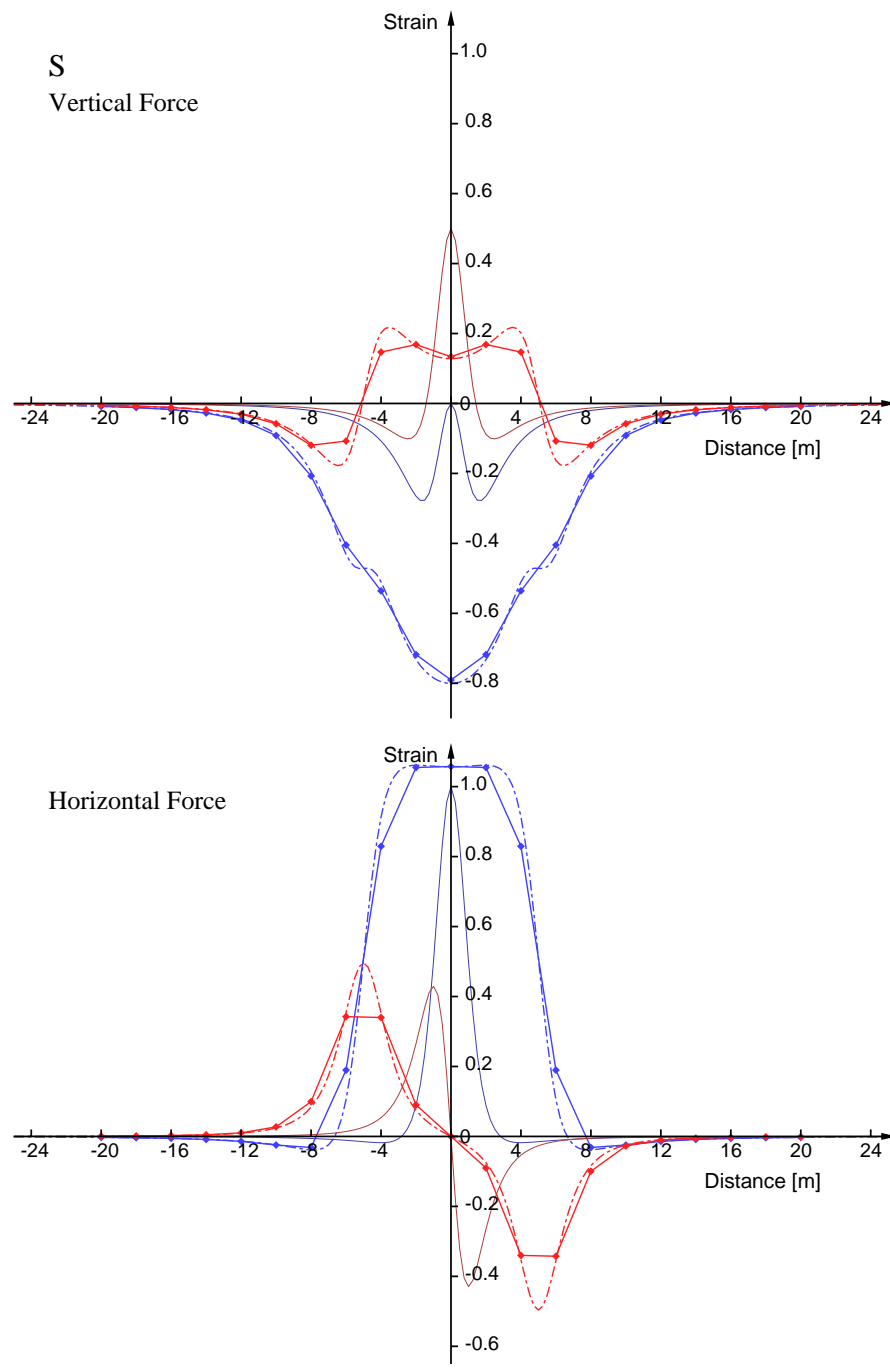


**Figure S3.** S wave DAS fields for a cable at 2 m depth with vertical and horizontal forces imposed at the origin. The traces are plotted with same convention as in Figure S2 with along cable in red and cross cable in blue.

6 *B.L.N. Kennett, V.H. Lai, M.S. Miller, D. Bowden, A. Fichtner*

## 1.2 Source to side of cable

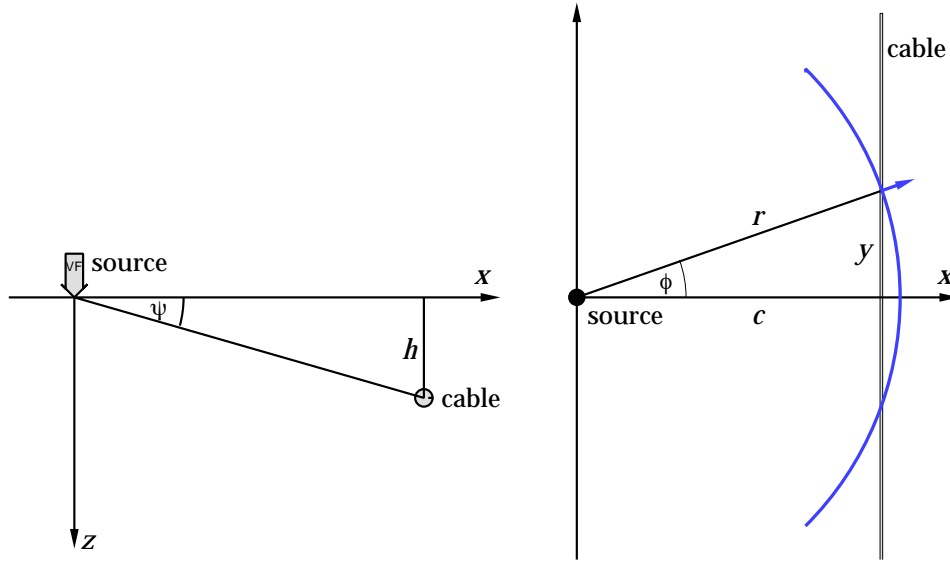


**Figure S4:** Configuration of shallow cable at depth  $h$  a horizontal distance  $c$  from the source at the origin. DAS recording is along the  $y$  direction.

For the scenario of a shallow cable close to a vertical force at the free surface, the displacement and strain field cannot be expressed in analytic form. However, these fields will have cylindrical symmetry around the source so that the outwardly directed radiation does not vary with azimuth. The fields will therefore depend on some function of radial distance  $r = (x^2 + y^2)^{1/2}$  (Figure S4). For the body wave component the dominant term in displacement decays as  $1/r$ , whereas for fully developed Rayleigh waves, with larger amplitude, the displacement depends on  $1/r^{1/2}$ . For a close cable, within a wavelength of the source for many frequencies, the Rayleigh waves are not completely established and the distance dependence is weak.

For a displacement field that depends on  $f(r)$ , the horizontal components at the point  $(x, y)$  are

$$u_x = \cos \phi f(r) = \frac{x}{r} f(r), \quad u_y = \sin \phi f(r) = \frac{y}{r} f(r). \quad (10)$$

The corresponding strains are given by

$$\begin{aligned} e_{xx} &= \frac{\partial}{\partial x} \left( \frac{x}{r} f(r) \right) = \frac{1}{r} \left( \frac{y^2}{r^2} f(r) + \frac{x^2}{r^2} [r f'(r)] \right) = \frac{1}{r} (\sin^2 \phi f(r) + \cos^2 \phi [r f'(r)]), \\ e_{yy} &= \frac{\partial}{\partial y} \left( \frac{y}{r} f(r) \right) = \frac{1}{r} \left( \frac{x^2}{r^2} f(r) + \frac{y^2}{r^2} [r f'(r)] \right) = \frac{1}{r} (\cos^2 \phi f(r) + \sin^2 \phi [r f'(r)]). \end{aligned} \quad (11)$$

where  $f'(r)$  is the derivative of  $f(r)$ . For a constant field  $f(r) = \text{const}$ , the strain dependence on the  $y$  coordinate, along the cable, depends on the functions  $g(r) = x^2/r^3$  and  $h(r) = y^2/r^3$ , which are illustrated in Figure S5, including the action of DAS gauge length integration and stacking.

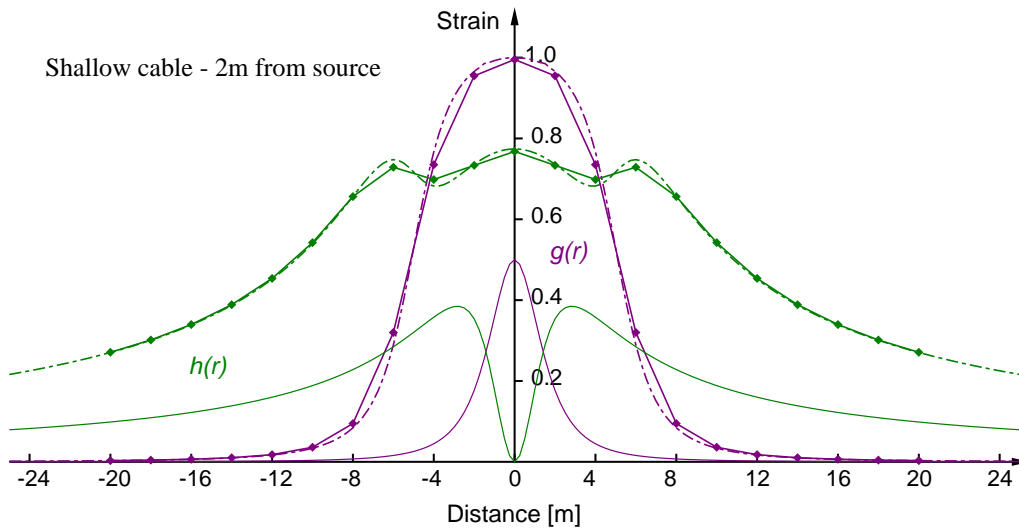


**Figure S5:** The basic functions  $g(r)$  and  $h(r)$  controlling the recorded DAS strain for a shallow cable for a source-cable separation of 2 m. The DAS signal traces are plotted with same convention as in Figure S2.

In addition to the horizontal strains, there will also be vertical strain for body waves, depending on  $\sin \psi$  (Figure S4). But, for Rayleigh waves near-surface vertical strain is very weak because the vertical displacement is almost constant with depth.

The spread of the wavefield from the source means that  $f(r)$  will decay with  $r$ , so that the basic functions  $g(r)$  and  $h(r)$  are further modulated by  $f(r)$  or  $r f'(r)$ . The specific pattern of strain dependence on offset  $y$  reflects the balance of the contributions in (11). Since for a decaying field  $r f'(r)$  will have the opposite sign to  $f(r)$ , there will be tendency for a change of sign with increasing offset.

In Figure S6 we show the along-cable dependence after DAS gauge length integration and stacking for  $f(r) = 1/r$  corresponding to body waves. The along-cable component shows zones of sign reversal as a function of offset. Such features can be seen in the DAS synthetics for near-offset presented by Kennett (2022). For this particular case, the across-cable response is simply the negative of that across cable, and so from the Poisson effect (equation 1 of main paper) gives a modest augmentation of amplitude.

In an urban environment exploiting ‘dark’ fibres the cable commonly runs along or beside streets, with buildings parallel to the cable run. Basements can act as strong reflectors for the seismic wavefield bringing in additional energy that appears to common from a ‘mirror’ virtual source on the far side of the reflector. The strain expression derived above can be used with the virtual source, but now the distance has to be measured from the mirror source location. For such longer paths Rayleigh waves will be more effectively developed, but will not yet have lost too much amplitude. Figure S7 shows the DAS strain response for a source-cable separation of 6 m, with an  $r^{-1/2}$  displacement decay, so

8 *B.L.N. Kennett, V.H. Lai, M.S. Miller, D. Bowden, A. Fichtner*

that the derivative term  $rf'(r)$  is  $-\frac{1}{2}r^{-1/2}$ . The along-cable DAS signal remains concentrated in the vicinity of the origin and the cross-cable term is weak.

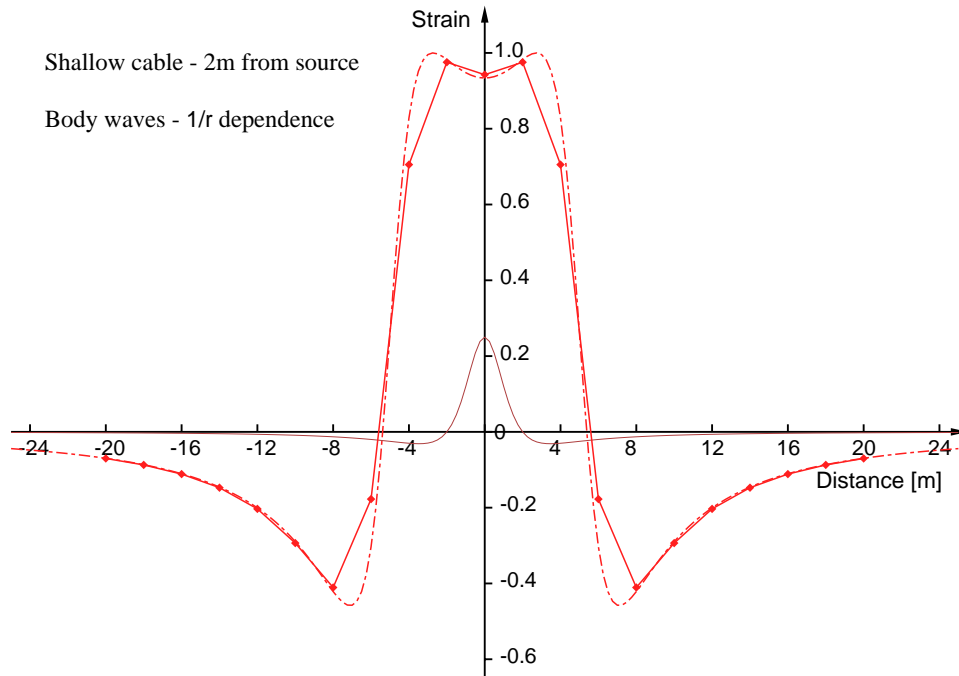


**Figure S6:** The along-cable DAS response for a  $1/r$  decay with a source-cable separation of 2 m. The traces are plotted with same convention as in Figure S2.

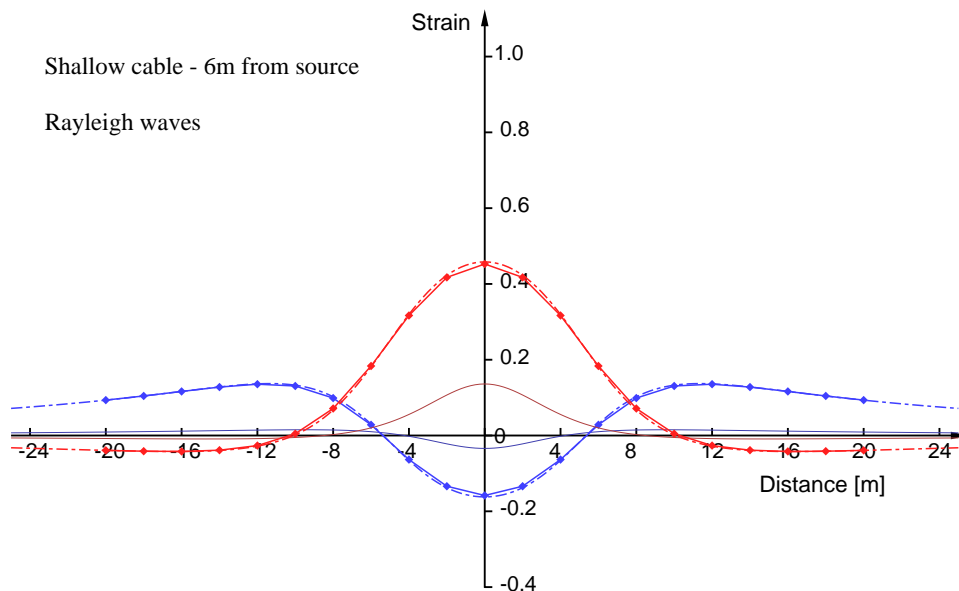


**Figure S7:** The DAS response for a  $1/r^{1/2}$  decay with a source-cable separation of 6 m. The traces are plotted with same convention as in Figure S2, with along cable in red and cross cable in blue.

## 2 EXPERIMENTAL CONFIGURATIONS

### 2.1 Tidbinbilla Tracking Station, Canberra, Australia

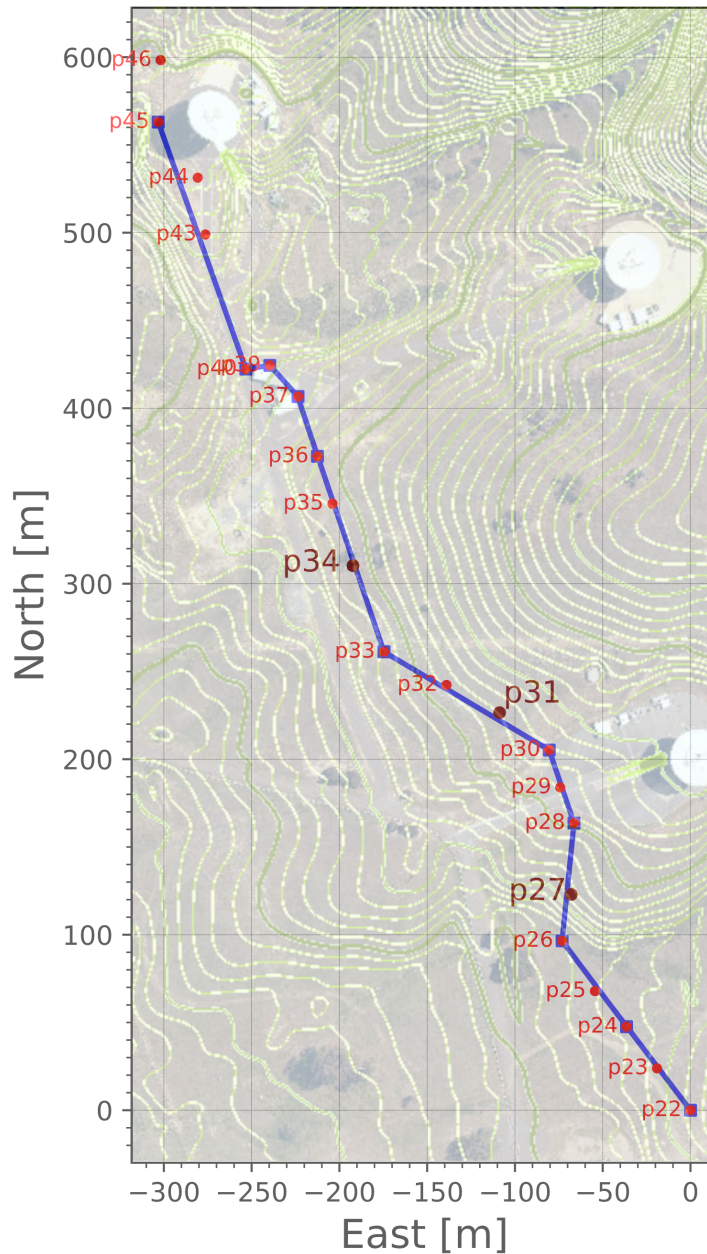


**Figure S8:** Layout of the experiment at the Tidbinbilla Tracking Station. the cable line is shown in blue and the maintenance pits as blue squares. The location of tap tests are shown in red. The three examples shown in Figures 5, 6 are indicated in larger type. The underlay shows 1 m contours from ACT interactive mapping (ACmapi 20203) superimposed on aerial photo mapping from 2021.

The experiment at the Tidbinbilla Deep Space Tracking Station near Canberra, operated by CSIRO, exploited dark fibre in the local communication network. The DAS system was attached to a loop of

10 *B.L.N. Kennett, V.H. Lai, M.S. Miller, D. Bowden, A. Fichtner*

fibres in the cable leading from the central building to a temporarily unused antenna dish to the north. Data were collected using a Silixa iDAS interrogator with 2 m channel spacing and a 10 m fixed gauge length and 1000 Hz sampling rate. The length of cable was approximately 1.9 km.

The map in Figure S8 shows the cable layout (black line), which trends southeast-northwest and emplaced in conduit at 2-metre depth, and the maintenance pits (black square) along the cable. Tap tests (marked as p22, p23 and so forth) are performed using a garden tamper to locate the channels and also extra cable loops in the maintenance pits.

The DAS array uses one of the fibres in the cable, starting from interrogator at the data server room (a few hundred metres southeast off the map) towards northwest, and connects to another fiber in the same cable at the antenna dish near p45 and returns to the data server room. As a result recordings are available for the tap tests from two different parts of the cable. Although there are some differences, probably related to the specific position of the different fibres in the cable, the results clearly indicate that the tap test response is associated with local conditions.

## 2.2 Bern Streets, Switzerland

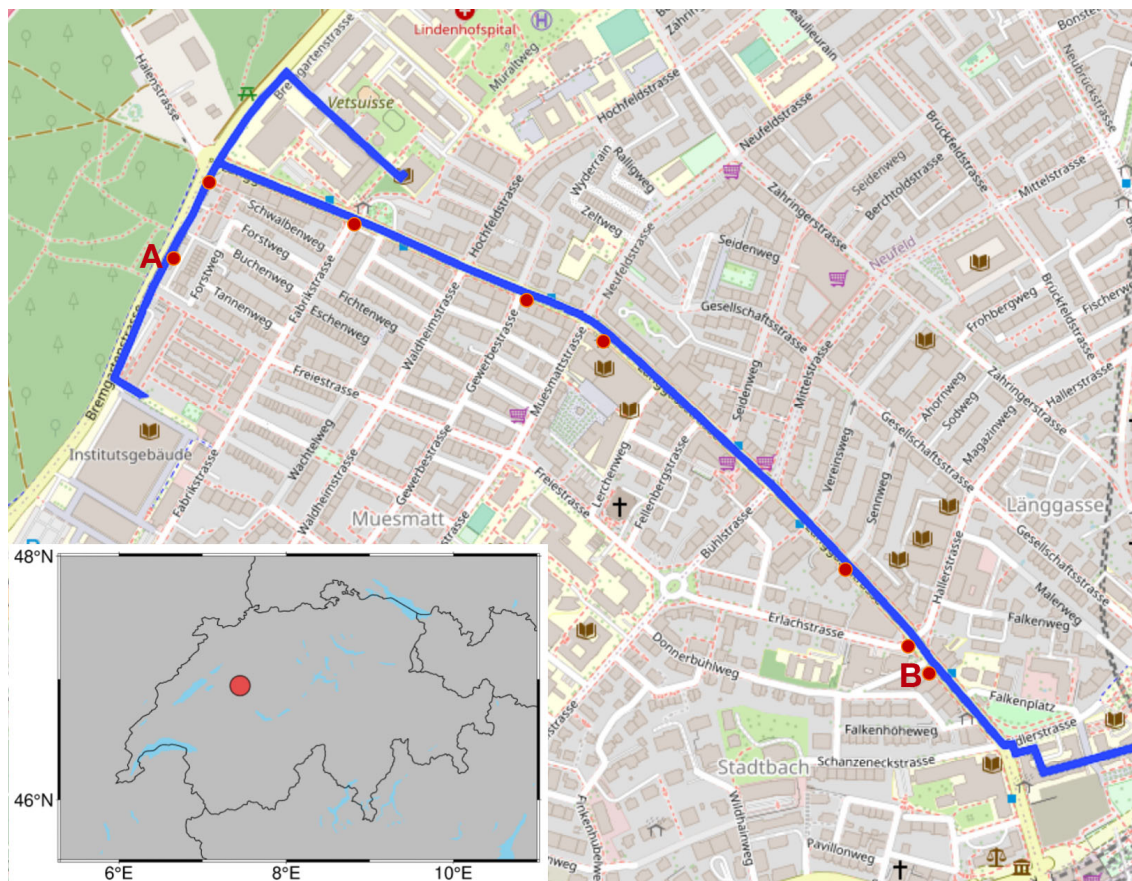


**Figure S9:** Layout of the DAS experiment along streets in Bern, Switzerland. The cable line is indicated in blue and the set of jump points are shown with red circles. The sites A and B illustrated in the main paper are indicated. Base map from Open Street Map.

This experiment along streets in the Länggasse area of Bern, Switzerland was carried out in November 2019. DAS seismic data was collected over a period of two weeks using existing telecommunication fibres connecting educational institutions, with access provided by the SWITCH Foundation.

The fibre layout consisted of around 3 km of fibre in a T-configuration (Figure S9), with the signal reflected at the far end. Data were collected using a Silixa iDAS interrogator, with 2 m channel spacing and a 10 m fixed gauge length. The data were extracted with a 200 Hz sampling rate.

The fibre optic cables are reported to be housed in a plastic conduit, buried at a depth of  $\sim 0.7$  m beneath the road. During construction, this conduit was covered with sand before the road surface was laid on top, and is likely to have been cemented in places (particularly near manholes).

The calibration of the DAS channels was carried out with a suite of jumps made by the same individual (DB) along the cable route on the edge of the sidewalk. The jump points are marked on Figure S9 by red circles. Such calibration is necessary because of the changes in conditions in the neighbourhood of inspection points spaced fairly regularly along the road. The DAS records show very low signal amplitude, and excess cable may be looped at the manholes.

The jump signals propagated to substantial distances (up to 40 m from the jump point) with clear initial P arrivals that allow the construction of a representative 1-D wavespeed profile along the street (Kennett, 2022). The jump sites A, B analysed in the main paper are marked in Figure S9.

The complex urban scenario with many buildings having substantial cellars extending to some depth means that there is complex situation with increase of seismic wavespeed with depth, but also the potential of shallow waveguide effects from the built environment.

### **3 RAYLEIGH WAVE REFLECTIONS**

In the Bern Street experiment many parts of the road are lined with buildings with cellars that can act as reflectors for shallow travelling energy such as Rayleigh waves. The configuration for a 16 m wide road with 2m sidewalks is shown to scale in Figure S10.

For such an experiment the DAS gauge length of 10 m is quite long compared to the distance from the building cellars and so even within the gauge length reflections occur at relatively wide angles. Strong reflection is to be expected at near-normal incidence but its effect will be spread by the DAS strain-rate averaging over at least the gauge length.

As noted in the main paper, the action of the reflection can be described in terms of virtual sources lying behind the reflector. This effect is illustrated in Figure S10 with dashed lines linking back from the reflected paths to a pink virtual source lying 2 m behind the reflecting wall.

In the Bern experiment, the Rayleigh wavespeed for the dominant frequencies is around 250 m/s. Thus, for a surface wave normally reflected on both sides of the road the delay would be approximately 0.125 s, which is consistent with the pattern of secondary arrivals seen for site B (figure 7 in main paper).

12 *B.L.N. Kennett, V.H. Lai, M.S. Miller, D. Bowden, A. Fichtner*

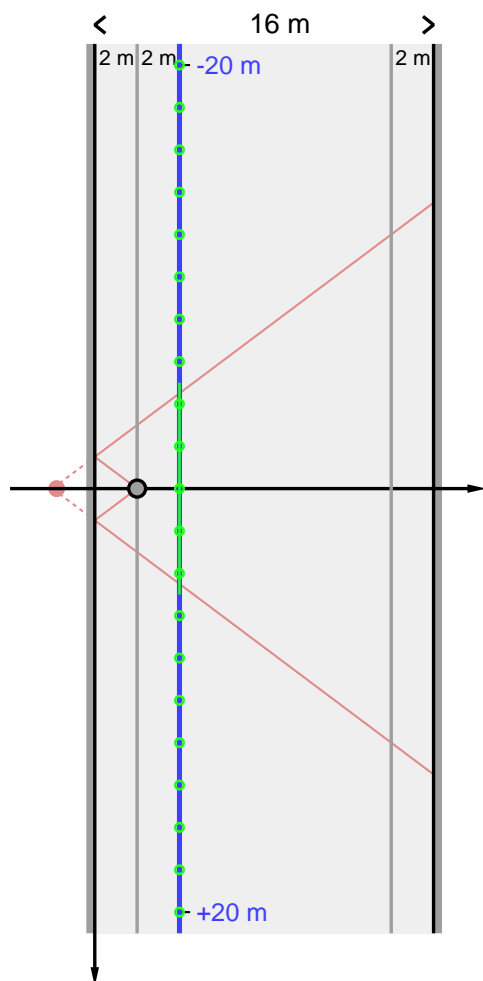


**Figure S10:** Scale diagram of the configuration of a DAS cable along a street – shown in blue. The jump point at the edge of the sidewalk is marked with a grey circle, 2m to the side of the cable. The position at which DAS channels are extracted is shown with green circles and the effect of a 10 m gauge length indicated by the green bar. The pink lines indicate the zone for which Rayleigh wave reflections will return within the gauge length of DAS sampling. The dashed lines pink link to the virtual source behind the reflector.

## REFERENCES

- ACTmapi, 2023. Australian Capital Territory interactive mapping, ACT Government, Canberra, Australia:  
<https://www.actmapi.act.gov.au>
- Aki, K. & Richards, P.G., 1980. *Quantitative Seismology*, W.H. Freeman, San Francisco.
- Kennett, B.L.N., 1983. *Seismic Wave Propagation in Stratified Media*, Cambridge University Press.
- Kennett, B.L.N., 2022. The seismic wavefield as seen by distributed acoustic sensing arrays: local, regional and teleseismic sources. *Proc. R. Soc. A*, **478**, 20210812. doi: 10.1098/rspa.2021.0812